

# Chromium solubility in anhydrous Phase B

Luca Bindi<sup>1,2</sup> · Ekaterina A. Sirotkina<sup>3,4</sup> · Andrey V. Bobrov<sup>3,4</sup> · Fabrizio Nestola<sup>5</sup> · Tetsuo Irifune<sup>6,7</sup>

Received: 17 June 2015 / Accepted: 24 August 2015  
© Springer-Verlag Berlin Heidelberg 2015

**Abstract** The crystal structure and chemical composition of a crystal of  $(\text{Mg}_{14-x}\text{Cr}_x)(\text{Si}_{5-x}\text{Cr}_x)\text{O}_{24}$  ( $x \approx 0.30$ ) anhydrous Phase B (Anh-B) synthesized in the model system  $\text{MgCr}_2\text{O}_4\text{--Mg}_2\text{SiO}_4$  at 12 GPa and 1600 °C have been investigated. The compound was found to be orthorhombic, space group *Pmcb*, with lattice parameters  $a = 5.900(1)$ ,  $b = 14.218(2)$ ,  $c = 10.029(2)$  Å,  $V = 841.3(2)$  Å<sup>3</sup> and  $Z = 2$ . The structure was refined to  $R_1 = 0.065$  using 1492 independent reflections. Chromium was found to substitute for both Mg at the M3 site (with a mean bond distance of 2.145 Å) and Si at the octahedral Si1 site (mean bond distance: 1.856 Å), according to the reaction  $\text{Mg}^{2+} + \text{Si}^{4+} = 2\text{Cr}^{3+}$ . Such substitutions cause a reduction in the volume of the M3 site and an increase in the volume of the Si-dominant octahedron with respect to the values typically observed for pure Anh-B and  $\text{Fe}^{2+}$ -bearing

Anh-B. Taking into account that  $\text{Cr}^{3+}$  is not expected to be Jahn–Teller active, it appears that both the  $\text{Cr}^{3+}$ –for–Mg and  $\text{Cr}^{3+}$ –for–Si substitutions in the Anh-B structure decrease the distortion of the octahedra. Electron microprobe analysis gave the  $\text{Mg}_{13.66(8)}\text{Si}_{4.70(6)}\text{Cr}_{0.62(4)}\text{O}_{24}$  stoichiometry for the studied phase. The successful synthesis of this phase provides new information for the possible mineral assemblages occurring in the Earth’s deep upper mantle and shed new light on the so-called X discontinuity that has been observed at 275–345 km depth in several subcontinental and subduction zone environments.

**Keywords** Anhydrous Phase B · Chromium · Upper mantle · X discontinuity · Crystal structure · Microprobe analysis · Synthesis

✉ Luca Bindi  
luca.bindi@unifi.it

- <sup>1</sup> Dipartimento di Scienze della Terra, Università di Firenze, Via La Pira 4, 50121 Florence, Italy
- <sup>2</sup> CNR - Istituto di Geoscienze e Georisorse, sezione di Firenze, Via La Pira 4, 50121 Florence, Italy
- <sup>3</sup> Department of Petrology, Geological Faculty, Moscow State University, Leninskie Gory, Moscow, Russia 119234
- <sup>4</sup> Vernadsky Institute of Geochemistry and Analytical Chemistry of Russian Academy of Sciences, Moscow, Russia 119991
- <sup>5</sup> Dipartimento di Geoscienze, Università di Padova, Via Gradenigo, 6, 35131 Padua, Italy
- <sup>6</sup> Geodynamics Research Center, Ehime University, Matsuyama 790-8577, Japan
- <sup>7</sup> Earth-Life Science Institute, Tokyo Institute of Technology, Tokyo 152-8550, Japan

## Introduction

Among the dense anhydrous magnesium silicates, anhydrous Phase B (Anh-B) has been first synthesized by Herzberg and Gasparik (1989). Later, Finger et al. (1989, 1991) reported its crystal structure and showed that it can be conveniently described as made of two types of layers: a layer with edge-sharing Mg and Si octahedra having the overall  $\text{Mg}_{12}\text{Si}_2\text{O}_{16}$  stoichiometry and a forsterite-type layer with Mg octahedra and Si tetrahedra having the overall  $\text{Mg}_{16}\text{Si}_8\text{O}_{32}$  stoichiometry.

In an experimental study on the stability of Anh-B, Ganguly and Frost (2006) showed that this phase might play a crucial role in the petrology of subducting slabs. This conflicts with the generally accepted view that with increasing pressure in the Earth’s mantle forsterite undergoes the transformation to wadsleyite and then to ringwoodite. Furthermore, Ganguly and Frost (2006) suggested that the

reaction forsterite + periclase to Anh-B could account for the so-called X discontinuity observed between 275 and 345 km below several subcontinental and subduction zone environments. This inferred reaction to produce Anh-B was also confirmed by ab initio calculations using the density functional method (Ottonello et al. 2010). If in fact Anh-B does form within the subducting slab, it could have significant consequences on seismic velocities and density structure of subducting slabs.

The role of minor elements incorporated into the Anh-B structure has only been studied by Hazen et al. (1992) who investigated Anh-B crystals synthesized at  $P = 15$  GPa and  $T = 1800$  °C that contained up to 1.68 a.p.f.u. of  $\text{Fe}^{2+}$  replacing Mg. However, to date, the effect of trivalent cations in the Anh-B structure has been not studied. The trivalent cations could enter the structure either by a  $\text{X}^{3+}$ -for-Mg substitution with the formation of oxygen vacancies or with a  $\text{X}^{3+}$ -for-Mg and  $\text{X}^{3+}$ -for-Si-coupled substitutions and would be expected to influence physical properties. Among the  $\text{X}^{3+}$  elements, chromium is believed to be a minor component in the primitive mantle (~0.3–0.4 wt%  $\text{Cr}_2\text{O}_3$ ; Ringwood 1979; Allègre et al. 1995; O'Neill and Palme 1998). Nevertheless, the crystal chemistry of high-pressure Cr-bearing phases under deep upper mantle conditions (e.g., Bindi et al. 2014a, 2014b, 2014c, 2015; Sirotkina et al. 2015) clearly needs to be established. The rationale for this is that in some cases, such a trivalent cation could increase the bulk modulus,  $K_{T0}$ . This is because the entry of Cr in diopside synthesized at high-pressure and temperature conditions has been shown by Boffa Ballaran et al. (2009) to strongly increase bulk modulus.

We have investigated phase relations in the model system  $\text{MgCr}_2\text{O}_4$ – $\text{Mg}_2\text{SiO}_4$  at 10–24 GPa and 1600 °C. The run product synthesized at  $P = 12$  GPa revealed the presence of crystalline materials having a mixed ( $\text{Mg}_{14-x}\text{Cr}_x$ ) ( $\text{Si}_{5-x}\text{Cr}_x$ ) $\text{O}_{24}$  ( $x \approx 0.30$ ) composition and exhibiting the Anh-B structure type. Here we report structural data obtained by single-crystal X-ray diffraction and also the chemical composition of this synthetic compound obtained by EDS and electron probe microanalysis.

## Methodology

### Synthesis

The experiment that produced run product 2627-40 was carried out at  $P = 12$  GPa and  $T = 1600$  °C using a 2000-t Kawai-type multi-anvil apparatus installed at the Ehime University (Matsuyama, Japan). Samples were compressed by eight cubic tungsten carbide anvils with 2.5-mm truncation edge lengths. Heating was performed by a tubular  $\text{LaCrO}_3$  heater. The samples were loaded into platinum

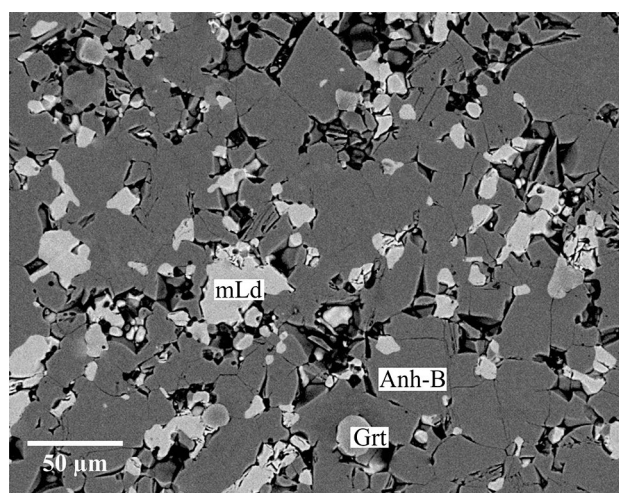


**Fig. 1** SEM-BSE image of idiomorphic crystals of the  $\text{Cr}^{3+}$ -bearing Anh-B phase studied here (Anh-B) associated with  $\text{Mg}_2\text{Cr}_2\text{O}_5$  (mLd) and garnet (Grt) in the run 2627-40 ( $P = 12$  GPa,  $T = 1600$  °C). CamScan electronic microscope MV2300

capsules and were isolated from the heater by an MgO insulator (Sirotkina et al. 2015). Approximate sample volumes after experiments were  $1.0 \text{ mm}^3$ . Mixtures of MgO,  $\text{SiO}_2$  and  $\text{Cr}_2\text{O}_3$  in stoichiometric proportions were used as starting materials and prepared for the composition magnesiochromite ( $\text{Sp-MgCr}_2\text{O}_4$ )–forsterite ( $\text{Fo-Mg}_2\text{SiO}_4$ )  $\text{Sp}_{10}\text{Fo}_{90}$  (mol%). Temperatures were measured by a  $\text{W}_{97}\text{Re}_3$ – $\text{W}_{75}\text{Re}_{25}$  thermocouple. The pressure was calibrated at room temperature using the semiconductor–metal transitions of Bi, ZnS and GaAs (Irifune et al. 2004). The effect of temperature on pressure was further corrected using the  $\alpha$ – $\beta$  and  $\beta$ – $\gamma$  phase transitions of olivine (Katsura and Ito 1989; Yamada et al. 2004). The run product comprised Cr-bearing Anh-B with  $\text{Mg}_2\text{Si}_2\text{O}_5$  (showing a modified ludwigite structure, hereafter labeled “mLd”) and majorite–knorringite garnet (Fig. 1). All the phases were identified by X-ray diffraction.

### Data collection and crystal-structure refinement

A small crystal ( $30 \times 35 \times 40 \text{ }\mu\text{m}$ ), handpicked under a reflected light microscope from run product 2627-40 (Fig. 1), was preliminarily examined with a Bruker-Enraf MACH3 single-crystal diffractometer using graphite-monochromatized  $\text{MoK}\alpha$  radiation. The data collection was then done with a Supernova (Rigaku-Oxford Diffraction) single-crystal diffractometer equipped with the Mova microsource (spot size  $0.120 \text{ mm}$ ,  $\text{MoK}\alpha$ ) and assembled with a Pilatus 200 K detector (Dectris) (see Table 1 for details). Intensity integration and standard Lorentz-polarization corrections were performed with the *CrysAlis* RED (Oxford Diffraction 2006) software package. The program

**Table 1** Details pertaining to the single-crystal X-ray data collection and structure refinement of Cr<sup>3+</sup>-bearing anhydrous Phase B

Crystal data	
Space group	<i>Pmcb</i> (#55)
Cell parameters	$a = 5.900(1) \text{ \AA}$ $b = 14.218(2) \text{ \AA}$ $c = 10.029(2) \text{ \AA}$ $V = 841.3(2) \text{ \AA}^3$
<i>Z</i>	2
Crystal color	Dark green
Crystal shape	Block
Crystal size (mm)	0.030 × 0.035 × 0.040
Data collection	
Diffractometer	Supernova (Rigaku–Oxford Diffraction)
Detector	Pilatus 200 K detector (Dectris)
Radiation type	MoK( $\lambda = 0.71073 \text{ \AA}$ )
Monochromator	Oriented graphite (002)
Scan mode	$\varphi/\omega$
Temperature (K)	298
Detector to sample distance (cm)	5
Number of frames	721
Rotation width per frame (°)	0.20
Measuring time (s)	50
Maximum covered $2\theta$ (°)	63.70
Range of $h, k, l$	$-7 \leq h \leq 8, -20 \leq k \leq 18,$ $-14 \leq l \leq 14$
Collected reflections	9009
$R_{\text{int}}$ before absorption correction	0.1125
$R_{\text{int}}$ after absorption correction	0.0767
Refinement	
Refinement coefficient	$F^2$
No. of refl. in refinement	1492
No. of observed refl.	911
No. of refined parameters	120
$R_1$ (obs)/ $R_1$ (all)	0.0412/0.0652
$S$ (obs)/ $S$ (all)	1.06/1.13
Diff. Fourier ( $e^{-\text{\AA}^{-3}}$ )	[−0.62, 0.87]

ABSPACK of the *CrysAlis* RED package (Oxford Diffraction 2006) was used for the absorption correction.

Reflection conditions ( $hk0: k = 2n; h0l: l = 2n; 0k0: k = 2n; 00l: l = 2n$ ) are consistent with the space group *Pmcb* (*Pbam* as standard), reported for Anh-B (Finger et al. 1989, 1991; Hazen et al. 1992). The full-matrix least-squares program SHELXL-97 (Sheldrick 2008), working on  $F^2$ , was used for the refinement of the structure, which was carried out starting from the atomic coordinates reported by Finger et al. (1991) for Anh-B. Site-scattering values were refined using scattering curves for neutral species (Ibers and Hamilton 1974) as follows: Mg vs. Cr for

the M sites, Si vs. Cr for the Si1 sites and O vs. □ (structural vacancy) for the anion sites. The O sites and all the M sites but M3 were found fully occupied, and the occupancy factors were then fixed to 1.00 (i.e., full occupancy of O and Mg, respectively). The refined mean electron numbers at the M3 and Si1 cation sites were found to be 15.6(2) and 16.9(1), respectively, thus indicating the same amount of Cr substituting for both Mg (at the M3 site) and Si (at the Si1 site). Successive cycles were run, introducing anisotropic temperature factors for all the atoms, leading to  $R_1 = 0.041$  for 911 observed reflections [ $F_o > 4\sigma(F_o)$ ] and  $R_1 = 0.065$  for all 1492 independent reflections. Fractional atomic coordinates and isotropic displacement parameters are shown in Table 2. Table 3 lists the anisotropic displacement parameters. Bond distances and bond valence sums are given in Tables 4 and 5, respectively.

### Chemical composition

A preliminary chemical analysis using energy-dispersive spectrometry, performed on the same crystal fragment used for the structural study as well as on other fragments from the same run product, did not indicate the presence of elements ( $Z > 9$ ) other than Cr, Mg and Si. The chemical composition was then determined using wavelength-dispersive analysis (WDS) by means of a JEOL JXA-8600 electron microprobe. We used 40 s as counting time. The matrix correction was performed with the Bence and Albee (1968) program as modified by Albee and Ray (1970). The standards employed were forsterite (Mg, Si) and synthetic Cr<sub>2</sub>O<sub>3</sub> (Cr). The crystal used for the X-ray study was found to be homogeneous within the analytical uncertainty. The average chemical composition (four analyses on different spots) is (wt%), SiO<sub>2</sub> 32.1(1); Cr<sub>2</sub>O<sub>3</sub> 5.37(6); MgO 62.6(3); total 100.1(3), corresponding, on the basis of 24 oxygen atoms, to Mg<sub>13.66(8)</sub>Si<sub>4.70(6)</sub>Cr<sub>0.62(4)</sub>O<sub>24</sub>.

### Results and discussion

The crystal structure of Cr<sup>3+</sup>-bearing Anh-B (Fig. 2) is basically identical to that of pure Mg<sub>14</sub>Si<sub>5</sub>O<sub>24</sub> (Finger et al. 1989, 1991) and Fe<sup>2+</sup>-bearing Anh-B (Hazen et al. 1992). It consists of a stacking of two types of layer parallel to the *b*-axis: (1) a defect rock-salt layer with edge-sharing M and Si octahedra involving the M1, M3, M4 and Si1 atoms and having the formula [Mg<sub>10</sub>(Mg<sub>0.70</sub>Cr<sub>0.30</sub>)<sub>2</sub>(Si<sub>0.70</sub>Cr<sub>0.30</sub>)<sub>2</sub>]O<sub>16</sub>, ideally Mg<sub>12</sub>Si<sub>2</sub>O<sub>16</sub>, and (2) a forsterite-type layer with M octahedra and Si tetrahedra involving the M2, M5, M6, Si2 and Si3 atoms and having the formula Mg<sub>16</sub>Si<sub>8</sub>O<sub>32</sub>. The number of atoms in the unit cell is thus Mg<sub>28</sub>Si<sub>10</sub>O<sub>48</sub> (ideal formula Mg<sub>14</sub>Si<sub>5</sub>O<sub>24</sub> with  $Z = 2$ ).

**Table 2** Atoms, Wyckoff positions, site occupation factors (s.o.f.), fractional atomic coordinates and equivalent isotropic displacement parameters ( $\text{\AA}^2$ ) for the selected crystal

Atom	Wyckoff	s.o.f.	x	y	z	$U_{\text{iso}}$
Si1	2a	Si <sub>0.71(2)</sub> Cr <sub>0.29</sub> <sup>3+</sup>	0.0000	0.0000	0.0000	0.0061(8)
Si2	4h	Si <sub>1.000</sub>	0.5000	0.31058(17)	0.8228(3)	0.0089(5)
Si3	4g	Si <sub>1.000</sub>	0.0000	0.37386(17)	0.0030(3)	0.0088(5)
M1	2d	Mg <sub>1.000</sub>	0.5000	0.0000	0.5000	0.0371(15)
M2	4h	Mg <sub>1.000</sub>	0.5000	0.1725(2)	0.6399(3)	0.0119(7)
M3	2b	Mg <sub>0.70(2)</sub> Cr <sub>0.30</sub> <sup>3+</sup>	0.5000	0.0000	0.0000	0.0060(10)
M4	8i	Mg <sub>1.000</sub>	0.2408(3)	−0.00109(14)	0.2582(2)	0.0064(5)
M5	4g	Mg <sub>1.000</sub>	0.0000	0.1778(2)	0.1793(3)	0.0083(6)
M6	8i	Mg <sub>1.000</sub>	0.7564(4)	0.16921(14)	0.9171(2)	0.0071(5)
O1	4g	O <sub>1.000</sub>	0.0000	0.0877(4)	0.3464(6)	0.0115(13)
O2	4g	O <sub>1.000</sub>	0.0000	0.0763(4)	0.8494(6)	0.0116(14)
O3	4g	O <sub>1.000</sub>	0.0000	0.2567(4)	0.0023(7)	0.0094(12)
O4	4h	O <sub>1.000</sub>	0.5000	0.0835(4)	0.8300(6)	0.0105(13)
O5	4h	O <sub>1.000</sub>	0.5000	0.4231(4)	0.8273(6)	0.0084(13)
O6	4h	O <sub>1.000</sub>	0.5000	0.2576(4)	0.9695(6)	0.0099(13)
O7	8i	O <sub>1.000</sub>	0.2298(8)	0.0897(3)	0.5801(4)	0.0120(10)
O8	8i	O <sub>1.000</sub>	0.7780(8)	0.0752(3)	0.0758(4)	0.0109(10)
O9	8i	O <sub>1.000</sub>	0.2829(8)	0.2597(3)	0.7507(5)	0.0099(9)

**Table 3** Anisotropic displacement parameters  $U_{ij}$  ( $\text{\AA}^2$ ) for the selected crystal

	$U^{11}$	$U^{22}$	$U^{33}$	$U^{12}$	$U^{13}$	$U^{23}$
Si1	0.0065(15)	0.0071(14)	0.0045(14)	0.000	0.000	0.0015(10)
Si2	0.0072(12)	0.0080(11)	0.0114(12)	0.000	0.000	0.0005(9)
Si3	0.0093(12)	0.0082(11)	0.0089(11)	0.000	0.000	0.0009(9)
M1	0.040(4)	0.039(3)	0.032(3)	0.000	0.000	0.000(3)
M2	0.0113(17)	0.0146(15)	0.0098(15)	0.000	0.000	0.0015(12)
M3	0.0028(17)	0.0065(16)	0.0088(16)	0.000	0.000	0.0012(11)
M4	0.0038(10)	0.0056(9)	0.0099(10)	−0.0002(8)	0.0010(8)	0.0010(7)
M5	0.0086(15)	0.0096(14)	0.0068(14)	0.000	0.000	0.0009(11)
M6	0.0065(11)	0.0070(9)	0.0080(10)	0.0003(8)	−0.0007(8)	0.0007(7)
O1	0.010(3)	0.014(3)	0.010(3)	0.000	0.000	−0.001(2)
O2	0.011(3)	0.014(3)	0.010(3)	0.000	0.000	−0.003(2)
O3	0.010(3)	0.005(3)	0.014(3)	0.000	0.000	0.000(2)
O4	0.011(3)	0.012(3)	0.009(3)	0.000	0.000	0.001(2)
O5	0.007(3)	0.008(3)	0.010(3)	0.000	0.000	0.001(2)
O6	0.012(3)	0.007(3)	0.011(3)	0.000	0.000	0.003(2)
O7	0.019(3)	0.0090(19)	0.008(2)	−0.0049(19)	−0.0028(19)	0.0028(17)
O8	0.012(2)	0.009(2)	0.012(2)	−0.0021(18)	−0.0033(19)	−0.0003(16)
O9	0.008(2)	0.010(2)	0.011(2)	0.0000(17)	−0.0011(19)	−0.0021(16)

As documented in previous studies (Finger et al. 1989, 1991; Hazen et al. 1992), the Si1 position (sixfold coordinated silicon) exhibits a peculiar crystallographic environment. Each octahedron shares all 12 edges with neighboring Mg octahedra and is, therefore, at the center of a 13 cation cluster (Fig. 3). However, the edge sharing between

different polyhedra is very limited. In detail, Si2 shares two edges with M octahedra, whereas Si3 shares only corners with the octahedra. Interestingly, the Si1 octahedron (site population: Si<sub>0.70</sub>Cr<sub>0.30</sub><sup>3+</sup>) is significantly larger (polyhedral volume: 8.55  $\text{\AA}^3$ ; Table 4) than that observed for pure Anh-B (7.85  $\text{\AA}^3$ ; Finger et al. 1991) and that in

**Table 4** Bond distances (Å) in the structure of Cr<sup>3+</sup>-bearing anhydrous Phase B

Si1-O8 (×4)	1.854(4)	M3-O4 (×2)	2.077(6)
Si1-O2 (×2)	1.860(7)	M3-O8 (×4)	2.100(4)
<Si1-O>	1.856	<M3-O>	2.145
V (Å <sup>3</sup> )	8.55	V (Å <sup>3</sup> )	11.91
σ <sup>2</sup>	0.03	σ <sup>2</sup>	58.03
λ	1.0000	λ	1.0165
Si2-O5	1.600(6)	M4-O5	2.012(4)
Si2-O9 (×2)	1.639(5)	M4-O7	2.054(5)
Si2-O6	1.652(7)	M4-O2	2.081(5)
<Si2-O>	1.633	M4-O1	2.096(5)
V (Å <sup>3</sup> )	2.19	M4-O4	2.120(5)
σ <sup>2</sup>	66.32	M4-O8	2.129(5)
λ	1.0146	<M4-O>	2.082
		V (Å <sup>3</sup> )	11.91
Si3-O7 (×2)	1.645(5)	σ <sup>2</sup>	24.50
Si3-O1	1.662(7)	λ	1.0075
Si3-O3	1.665(6)		
<Si3-O>	1.654	M5-O9 (×2)	2.022(5)
V (Å <sup>3</sup> )	2.33	M5-O3	2.100(7)
σ <sup>2</sup>	1.05	M5-O1	2.110(7)
λ	1.0003	M5-O8 (×2)	2.219(5)
		<M5-O>	2.115
M1-O5 (×2)	2.048(6)	V (Å <sup>3</sup> )	12.22
M1-O7 (×4)	2.194(5)	σ <sup>2</sup>	74.96
<M1-O>	2.145	λ	1.0226
V (Å <sup>3</sup> )	13.09		
σ <sup>2</sup>	3.64	M6-O6	2.036(5)
λ	1.0031	M6-O2	2.066(5)
		M6-O8	2.083(5)
M2-O6	1.977(7)	M6-O3	2.085(5)
M2-O7 (×2)	2.070(5)	M6-O9	2.120(5)
M2-O9 (×2)	2.101(5)	M6-O4	2.130(5)
M2-O4	2.289(7)	<M6-O>	2.087
<M2-O>	2.101	V (Å <sup>3</sup> )	11.78
V (Å <sup>3</sup> )	12.08	σ <sup>2</sup>	65.78
σ <sup>2</sup>	57.66	λ	1.0190
λ	1.0179		

Fe<sup>2+</sup>-bearing Anh-B (7.82 Å<sup>3</sup>; Hazen et al. 1992), in keeping with the presence of the bigger Cr<sup>3+</sup> cation. Such an enlargement reduces the lattice strain of the close-packed O array in the vicinity of the 12 shared O–O edges (Fig. 3) and allows the Cr<sup>3+</sup>-for-Mg substitution at the M3 site. A similar but reversed situation was observed for Fe<sup>2+</sup>-bearing Anh-B (Hazen et al. 1992). The octahedral site hosting the greatest amount of Fe<sup>2+</sup> is M3, which, with

its enlargement, compensates the reduction in size due the presence of octahedral silicon. Si1 and M3 octahedra, indeed, form edge-sharing strips parallel to the *a* crystallographic axis. Thus, it seems that the M3 octahedron plays a crucial role in the Anh-B structure to accomplish the required size compensation.

Taking into account that Cr<sup>3+</sup> is not expected to be Jahn–Teller active, it appears that the Cr<sup>3+</sup>-for-Si and Cr<sup>3+</sup>-for-Mg substitutions also induce a regularization of the octahedral sites quantifiable with a decrease in the octahedral angle variance σ<sup>2</sup> (Robinson et al. 1971) with respect to pure Anh-B and Fe<sup>2+</sup>-bearing Anh-B. The decrease in the octahedral angle variance σ<sup>2</sup> is especially marked for M3: 58.03 in Cr<sup>3+</sup>-bearing Anh-B (this study), 82.34 in Anh-B (Finger et al. 1991) and 90.79 in Fe<sup>2+</sup>-bearing Anh-B (Hazen et al. 1992).

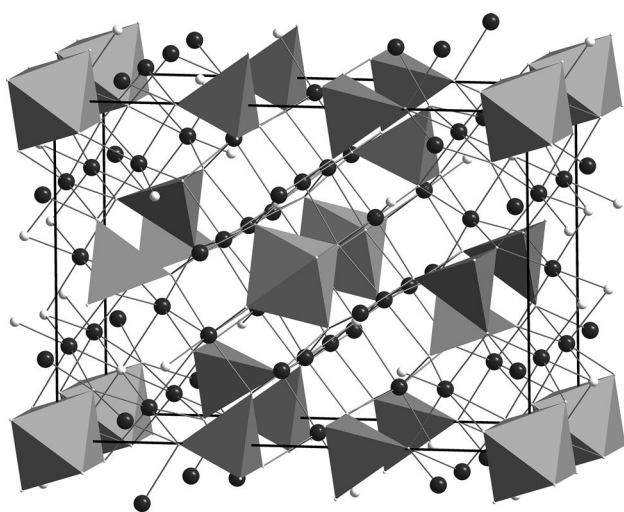
As expected, the unit-cell parameters of Cr<sup>3+</sup>-bearing Anh-B are intermediate between those measured for pure Anh-B [*a* = 5.868(1), *b* = 14.178(1), *c* = 10.048(1) Å; Finger et al. 1991] and those observed for Fe<sup>2+</sup>-bearing Anh-B [*a* = 5.908(2), *b* = 14.241(3), *c* = 10.069(3) Å; Hazen et al. 1992]. The enlargement, induced by the Cr<sup>3+</sup>-for-Si substitution, is counterbalanced by the Cr<sup>3+</sup>-for-Mg replacement.

The bond valence sums (Table 5) calculated using the parameters given by Brese and O’Keeffe (1991) corroborate both the trivalent state for Cr and the proposed cation distribution at the structural sites.

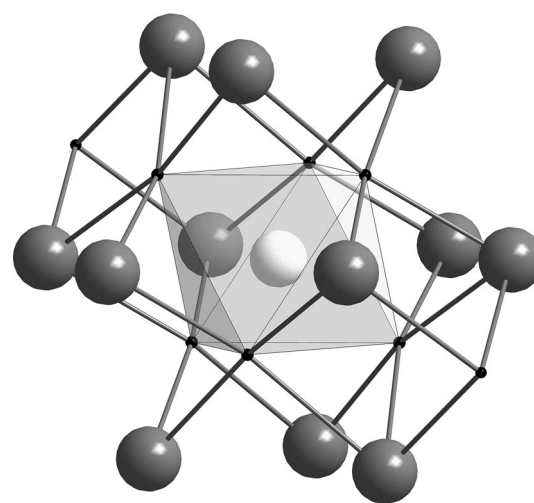
According to the geophysical and experimental data, the Earth’s mantle mineralogy is mostly based on phase relations in the system MgO–SiO<sub>2</sub> whose components account for ~88 mol% of mantle phases (Ringwood 1979). Although Fe substitutes easily for Mg in olivine pyroxene, garnet, wadsleyite and other silicates within the spinel, ilmenite and perovskite structures, phase equilibria in the Fe-free silicate system are often applied to the whole mantle with Mg/(Mg + Fe) of ~0.9. Ganguly and Frost (2006) suggested the possibility of the formation of anhydrous Phase B in the sequence of Wad → Anh-B + Sti → Rin (1 in Fig. 4), instead of the direct transformation of wadsleyite to ringwoodite, within some cold oceanic slabs. This may cause an eye-shaped splitting of the 410-km discontinuity within the interior of a cold slab. In addition, olivine could react with periclase (MgO) in a relatively silica-deficient portion of the mantle to form Anh-B (Fo + Per → Anh-B; 2 in Fig. 4), and this may explain the so-called X discontinuity that has been observed at 275–345 km depth in several subcontinental and subduction zone environments (Revenaugh and Williams 2000; Ganguly and Frost 2006).

**Table 5** Bond valence calculation (in *v.u.*) for the structure of Cr<sup>3+</sup>-bearing anhydrous Phase B

	Si1	Si2	Si3	M1	M2	M3	M4	M5	M6	$\Sigma$ O
	Si <sub>0.70</sub> Cr <sub>0.30</sub>	Si	Si	Mg	Mg	Mg <sub>0.70</sub> Cr <sub>0.30</sub>	Mg	Mg	Mg	
O1			0.942				0.336 <sup>×2→</sup>	0.324		1.938
O2	0.594 <sup>×2↓</sup>						0.350 <sup>×2→</sup>		0.365 <sup>×2→</sup>	2.024
O3			0.935					0.333	0.347 <sup>×2→</sup>	1.962
O4					0.200	0.363 <sup>×2↓</sup>	0.315 <sup>×2→</sup>		0.307 <sup>×2→</sup>	1.807
O5		1.111		0.383 <sup>×2↓</sup>			0.422 <sup>×2→</sup>			2.338
O6		0.965			0.464				0.396 <sup>×2→</sup>	2.221
O7			0.987 <sup>×2↓</sup>	0.258 <sup>×4↓</sup>	0.361 <sup>×2↓</sup>		0.377			1.983
O8	0.604 <sup>×4↓</sup>					0.342 <sup>×4↓</sup>	0.308	0.241 <sup>×2↓</sup>	0.349	1.844
O9		1.003 <sup>×2↓</sup>			0.332 <sup>×2↓</sup>			0.411 <sup>×2↓</sup>	0.315	2.061
	3.604	4.082	3.851	1.798	2.050	2.094	2.108	1.961	2.079	

**Fig. 2** The crystal structure of Cr<sup>3+</sup>-bearing Anh-B projected down [100] (perspective view). Si1 (Si,Cr), Si2 and Si3 cations are depicted as *dark gray* polyhedra, respectively, whereas the M cations and O atoms as *black* and *white* spheres, respectively. The unit cell is *outlined*. The vertical axis is the *b*-axis

The appearance of Anh-B in the Cr-bearing system under the conditions of the lowermost upper mantle is rather important since this phase associates with majorite–knorringite garnet that is a phase of the peridotitic assemblage of inclusions in natural diamonds (Stachel 2001). This association (plus Si-bearing Mg<sub>2</sub>Cr<sub>2</sub>O<sub>5</sub> with a mLd structure) was produced using a starting material Mg<sub>2</sub>SiO<sub>4</sub> (60 mol%) + MgCr<sub>2</sub>O<sub>4</sub> (40 mol%) at 12 GPa and 1600 °C (Bindi et al. 2015). It is notable that garnet in our runs contains 50–75 mol% knorringite and its composition is controlled by the composition of the starting material. As it is evident in Fig. 4, the composition of the starting material

**Fig. 3** Coordination environment of the Si1 octahedron in the crystal structure of Cr<sup>3+</sup>-bearing Anh-B. The M cations are drawn as *gray spheres* for clarity

required for the appearance of the Grt + Anh-B association should plot in the Grt–Anh-B–mLd triangle, so that the lowest magnesiochromite (MChr) content in the starting material should be 10 mol% (9.8 wt% Cr<sub>2</sub>O<sub>3</sub>). According to Kesson and Ringwood (1989), the protolith of the knorringite-rich garnet association may form as a residue of partial melting in the spinel peridotite stability field. Cr-rich garnets would crystallize from such compositions during subduction into the garnet stability field. Although it is not possible to estimate the likely maximum chromium content in the protolith of knorringite-rich garnet associations, a possible constraint could be provided by the compositions of the most Cr-rich garnets observed to date (20 wt% Cr<sub>2</sub>O<sub>3</sub>) as inclusions in diamonds (Stachel and Harris 1997). This

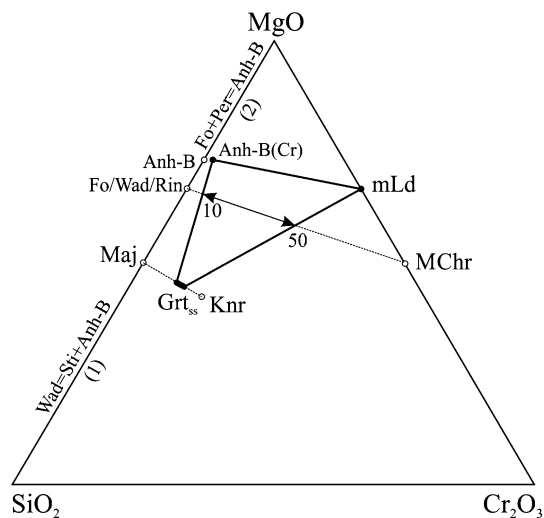


**Fig. 4** The relative position of phases within the triangle  $\text{SiO}_2$ – $\text{MgO}$ – $\text{Cr}_2\text{O}_3$ . Solid lines indicate the phase assemblage (Anh-B + Grt + mLD) synthesized in our run at 12 GPa and 1600 °C. Dashed lines indicate the studied system ( $\text{Mg}_2\text{SiO}_4$ – $\text{MgCr}_2\text{O}_4$ ) and garnet solid solution ( $\text{Grt}_{\text{ss}}$ ) on the khorringite–majorite series. Arrows denote the compositional range (10–50 mol%  $\text{MgCr}_2\text{O}_4$ ), in which the garnet–Anh-B phase assemblage may be formed. (1) and (2) are the two major reactions for Cr-free Anh-B phase formation

observation has implications for the results obtained in our study which show that Cr-bearing Anh-B may be found as inclusions in natural diamonds formed in Cr-rich mantle protolith (deeply subducted Cr-rich oceanic lithosphere) in the lowermost upper mantle and transition zone. This is an important observation and to obtain the data on the stability of Cr-bearing Anh-B, and other mantle phases enriched in Cr experiments in the  $\text{Mg}_2\text{SiO}_4$ – $\text{MgCr}_2\text{O}_4$  system should be continued in a wide pressure range.

**Acknowledgments** The manuscript took advantage from the revision of Kenneth Collerson and Sabrina Nazzareni. The research was supported by “progetto di Ateneo 2013, University of Firenze” to LB, by C.N.R., Istituto di Geoscienze e Georisorse sezione di Firenze, Italy, the Russian Foundation for Basic Research (Project No. 15-55-50033 YaF) to ES and AB. ES thanks Geodynamics Research Center, Ehime University, Matsuyama, Japan, for support of her visit in 2014. FN thanks the ERC Starting Grant 2012 (Grant agreement No. 307322).

## References

Albee AL, Ray L (1970) Correction factors for electron probe analysis of silicate, oxides, carbonates, phosphates, and sulfates. *Anal Chem* 48:1408–1414

Allègre JA, Poirier JP, Humler E, Hofmann AW (1995) The chemical composition of the Earth. *Earth Plan Sci Lett* 134:515–526

Bence AE, Albee AL (1968) Empirical correction factors for the electron microanalysis of silicate and oxides. *J Geol* 76:382–403

Bindi L, Sirotkina E, Bobrov AV, Irifune T (2014a) Chromium solubility in perovskite at high pressure: the structure of  $(\text{Mg}_{1-x}\text{Cr}_x)\text{O}_3$  (with  $x = 0.07$ ) synthesized at 23 GPa and 1600 C. *Am Miner* 99:866–869

Bindi L, Sirotkina E, Bobrov AV, Irifune T (2014b) X-ray single-crystal structural characterization of  $\text{MgCr}_2\text{O}_4$ , a post-spinel phase synthesized at 23 GPa and 1600 C. *J Phys Chem Solids* 75:638–641

Bindi L, Sirotkina E, Bobrov AV, Irifune T (2014c) Chromium solubility in  $\text{MgSiO}_3$  ilmenite at high pressure. *Phys Chem Minerals* 41:519–526

Bindi L, Sirotkina E, Bobrov AV, Irifune T (2015) Structural and chemical characterization of  $\text{Mg}[(\text{Cr}, \text{Mg})(\text{Si}, \text{Mg})\text{O}_4]$ , a new post-spinel phase with sixfold-coordinated silicon. *Am Miner* 100:1633–1636

Boffa Ballaran T, Nestola F, Tribaudino M, Ohashi H (2009) Bulk modulus variation along the diopside–kosmochlor solid solution. *Eur J Mineral* 21:591–597

Breese NE, O’Keeffe M (1991) Bond-valence parameters for solids. *Acta Crystallogr B* 47:192–197

Finger LW, Ko J, Hazen RM, Gasparik T, Hemley RJ, Prewitt CT, Weidner DJ (1989) Crystal chemistry of Phase B and an anhydrous analogue: implications for water storage in the upper mantle. *Nature* 341:140–142

Finger LW, Hazen RM, Prewitt CT (1991) Crystal structures of  $\text{Mg}_{12}\text{Si}_4\text{O}_{19}(\text{OH})_2$  (Phase B) and  $\text{Mg}_{14}\text{Si}_5\text{O}_{24}$  (phase AnhB). *Am Miner* 76:1–7

Ganguly J, Frost DJ (2006) Stability of anhydrous Phase B: experimental studies and implications for phase relations in subducting slab and the X discontinuity in the mantle. *J Geophys Res* 111:B06203

Hazen RM, Finger LW, Ko J (1992) Crystal chemistry of Fe-bearing anhydrous Phase B: implications for transition zone mineralogy. *Am Miner* 77:217–220

Herzberg C, Gasparik T (1989) Melting experiments on chondrite at high pressures: stability of anhydrous Phase B. *Eos* 70:484

Ibers JA, Hamilton WC (eds) (1974) *International Tables for X-ray crystallography*, vol IV. Kynock, The Netherlands, p 366

Irifune T, Kurio A, Sakamoto S, Inoue T, Sumiya H, Funakoshi K (2004) Formation of pure polycrystalline diamond by direct conversion of graphite at high pressure and high temperature. *Phys Earth Planet Inter* 143–144:593–600

Katsura T, Ito E (1989) The system  $\text{Mg}_2\text{SiO}_4$ – $\text{Fe}_2\text{SiO}_4$  at high pressure and temperatures: precise determination of stabilities of olivine, modified spinel, and spinel. *J Geophys Res* 94:15663–15670

Kesson SE, Ringwood AE (1989) Slab–mantle interactions 2. The formation of diamonds. *Chem Geol* 78:97–118

O’Neill HStC, Palme H (1998) Composition of the silicate earth: implications for accretion and core formation. In: Jackson I (ed) *The Earth’s mantle–composition, structure and evolution*. Cambridge University Press, U.K., pp 3–126

Otonello G, Civalleri B, Ganguly J, Perger WF, Belmonte D, Vetuschi Zuccolini M (2010) Thermo-chemical and thermo-physical properties of the high-pressure phase anhydrous B ( $\text{Mg}_{14}\text{Si}_5\text{O}_{24}$ ): an ab initio all-electron investigation. *Am Miner* 95:563–573

Oxford Diffraction (2006) *CrysAlis RED* (Version 1.171.31.2) and *ABSPACK* in *CrysAlis RED*. Oxford Diffraction Ltd, Abingdon, Oxfordshire, England

Revenaugh J, Williams Q (2000) The seismic X discontinuity: Observations and modeling. *Eos Trans. AGU*, 81(48), Fall Meet. Suppl., Abstract S21E – 05

Ringwood AE (1979) *Origin of the Earth and Moon*. Springer, New York

Robinson K, Gibbs GV, Ribbe PH (1971) Quadratic elongation: a quantitative measure of distortion in coordination polyhedra. *Science* 172:567–570

Sheldrick GM (2008) A short history of SHELX. *Acta Crystallogr A* 64:112–122

- Sirotkina EA, Bobrov AV, Bindi L, Irifune T (2015) Phase relations and formation of chromium-rich phases in the system  $\text{Mg}_4\text{Si}_4\text{O}_{12}$ – $\text{Mg}_3\text{Cr}_2\text{Si}_3\text{O}_{12}$  at 10–24 GPa and 1600 C. *Contr Min Petr* 169:2
- Stachel T (2001) Diamonds from the asthenosphere and the transition zone. *Eur J Min* 13:883–892
- Stachel T, Harris JW (1997) Diamond precipitation and mantle metasomatism-evidence from the trace element chemistry of silicate inclusions in diamonds from Akwatia, Ghana. *Contr Mineral Petrol* 129:143–154
- Yamada A, Inoue T, Irifune T (2004) Melting of enstatite from 13 to 18 GPa under hydrous conditions. *Phys Earth Planet Inter* 147:45–56